Undoped and Li-Doped NiO Coral Reef-like Structures Fabricated using Immersion Method

Nor Amirah Ladjahirin [1], *Norfarariyanti* Parimon[2*], *Mohamad Hafiz* Mamat[3,4], *Mohd Firdaus* Malek[4,5], and *Muhammad Nur Afnan* Uda[1]

[1]Faculty of Engineering, Universiti Malaysia Sabah, Jalan UMS, 88400 Kota Kinabalu, Sabah, Malaysia
[2]Centre of Research in Energy and Advanced Materials (CREAM), Faculty of Engineering, Universiti Malaysia Sabah, Jalan UMS, 88400 Kota Kinabalu, Sabah, Malaysia
[3]NANO-ElecTronic Centre (NET), School of Electrical Engineering, College of Engineering, Universiti Teknologi MARA, 40450 Shah Alam, Selangor, Malaysia
[4]NANO-SciTech Lab (NST), Centre for Functional Materials and Nanotechnology, Institute of Science (IOS), Universiti Teknologi MARA, 40450 Shah Alam, Selangor, Malaysia
[5]Faculty of Applied Sciences, Universiti Teknologi MARA, 40450 Shah Alam, Selangor, Malaysia

Abstract. Nickel oxide (NiO) is one of the p-type semiconductors with unique properties suitable for nanosensor applications. It has a wide range band gap and can be fabricated in various methods, leading to different nanostructures and results. In this study, undoped and lithium (Li)-doped NiO were fabricated using the immersion method to investigate their properties. The field emission scanning electron microscopy analysis revealed that both samples produced two layers of nanosheet and nano coral reef-like (CR) structures. X-ray diffraction patterns confirmed the average crystallite sizes for undoped and Li-doped NiO are 24.70 nm and 31.19 nm, respectively. According to ultraviolet-visible spectroscopy, Li-doped NiO has a higher average transmittance percentage of 53% compared to undoped NiO, which has 40%. The estimated optical band gap values are not much different, with 3.94 eV for undoped and 3.95 eV for Li-doped. Electrical measurements also indicated that Li-doped NiO has a higher conductivity value of 7.9 x 10^{-2} S.m^{-1}, whereas undoped NiO has 7.71 x 10^{-2} S.m^{-1}.

1 Introduction

The silicon nanosensor-based industry has experienced increased demand in past years due to their reliability. However, over time, researchers explored other alternatives to develop sensors that can match the performance of silicon-based sensors. One such option is the use of metal oxide semiconductors (MOSs). MOS-based sensors are susceptible and can detect even small changes in the environment, such as the detection of harmful and toxic gases [1]. Moreover, they are inexpensive to manufacture, making them an affordable solution for many applications.

* Corresponding author: fara2012@ums.edu.my

Generally, there are two types of MOSs, which are n-type and p-type. In recent years, several n-type metal oxides have gained popularity in research, such as indium (III) oxide (In_2O_3), zinc oxide (ZnO), titanium dioxide (TiO_2), and tin (IV) oxide (SnO_2), which have been studied extensively for their properties and potential applications. On the other hand, p-type metal oxides are less common, but they are still a crucial area of research. Several different materials have been identified as potential p-type semiconductors, including nickel oxide (NiO), copper oxide (CuO), copper (II) oxide (Cu_2O), tin (II) oxide (SnO), and cobalt oxide (Co_3O_4). These materials are characterized by their ability to conduct holes essentially, the absence of electrons, which makes them useful in various applications, such as sensors and energy conversion devices.

NiO is widely used by researchers due to its exceptional characteristics. This material is used in various fields, such as battery cathodes [2], solar cells [3], electrochromic coatings [4], antiferromagnetic materials [5], smart windows [6], and supercapacitors [7], due to its remarkable properties such as having a wide band gap ranging between 3.6 to 4.0 eV. The surface area, color, and nonstoichiometric levels of NiO samples can vary depending on the preparation conditions [8]. Due to these properties, many researchers have studied the impact of NiO samples on the morphological, electrical, structural, and optical properties in sensor fields and energy conversion devices. Most researchers suggest that dopants can be added to NiO samples to enhance the NiO performance. Doping is a prevalent technique used in semiconductor fabrication to modify the behavior and conductivity of the samples by introducing extra electrons or electron holes into the precursor samples. According to Wang et al. [9], even small amounts of dopant atoms can significantly alter the sensitivity of the samples and improve their sensing performance. A few transition metals have been employed as dopants in NiO. For example, Ahmed et al. used zinc (Zn) and manganese (Mn) to be doped with NiO through a co-precipitation method for optoelectronic application purposes [10]. On the other hand, Ahmed et al. fabricated chromium (Cr)-doped NiO forming nanorod structures for supercapacitor application, while Sahoo et al. suggested doping NiO with copper (Cu) to be used for photocathodes in water splitting applications [7, 11].

In this study, besides undoped NiO, lithium (Li) is used as a dopant element to be incorporated with NiO. The immersion method is employed to deposit undoped and Li-doped NiO nanostructures, with a NiO thin film (TF) used to enhance the adhesion between the nanostructures and glass substrates, as previous research has confirmed [12].

2 Methodology

2.1 Experimental work

Firstly, a thin film (TF) of NiO is deposited on two glass substrates using a sol-gel spin coating to enhance the adhesion of undoped and Li-doped NiO nanostructures, respectively. 0.5 M nickel acetate (II) tetrahydrate is dissolved into the mixture of 2 ml diethanolamine and 50 ml 2-methoxyethanol before being stirred at 500 rpm for 24 hours at 30 °C. Then, the well-stirred solution goes through the 5000 rpm spin coating process, where 10 drops of the solution are dropped onto the spinning glass before drying for 5 min. The process is repeated for another four layers. The final step is annealing the TFs for 3 h at a temperature of 500 °C.

The second process is the growth of NiO nanostructures, which are undoped and Li-doped NiO. 0.2 M of nickel (II) nitrate hexahydrate is dissolved into the mixture of 0.2 M hexamethylenetetramine and 100 ml deionized (DI) water. For growing the Li-doped NiO nanostructure, 1 at.% of lithium acetate dihydrate is added into the solution. The solution is sonicated for 1 h and stirred for 1.5 h at 500 rpm. Through the sonication process, the solid

particles in the solution will break down and disperse in a solvent to achieve a uniform solution mixture. The solution is poured into Schott bottles, where the NiO TF-coated glass substrate inside faces upwards. The bottles were then immersed in a water bath at 95 °C for 2 h to grow the nanostructures on the NiO TF. After immersion, the samples were rinsed thoroughly with DI water and dried for 20 min at 150 °C. They were then annealed for 1 h at a temperature of 500 °C.

2.2 Characterization

The surface morphology and cross-sectional images of the undoped and Li-doped NiO samples were examined using a field emission scanning electron microscope (FESEM) model Hitachi SU8020.

The crystal properties were determined through X-ray diffraction (XRD) patterns. These patterns were analyzed using an X-ray diffractometer Rigaku Model Ultima IV. From these patterns, various properties such as full width at half maximum (FWHM), dislocation density (δ), interplanar spacing (d), lattice parameters (a), unit cell volume (V), strain (ε), and stress (σ) can be obtained. The average crystallite size (D) was assessed using the Debye-Scherrer (1) relation [13].

$$D = \frac{k\lambda}{\beta \cos \theta} \tag{1}$$

where k is the constant value of 0.94, λ is the X-ray wavelength with a value of 1.542 Å, β is the FWHM in radians, and θ is the diffraction angle in degree.

Both undoped and Li-doped NiO samples were analyzed for their optical properties through an ultraviolet-visible spectrometer (UV-vis) model Jasco/V-670 EX. The analysis was carried out in the 300 - 800 nm wavelength range. The optical band gap (E_g) was determined from the transmittance plot. The absorption coefficient (α) was calculated using Lambert's law, as shown in (2).

$$\alpha = \frac{1}{t} \ln \frac{1}{T} \tag{2}$$

where t and T represent the thickness and transmittance of the film. Then, the E_g of undoped and Li-doped NiO was estimated by employing the Tauc model referring to the Davis and Mott relation [14] as shown in (3):

$$(\alpha h\nu)^2 = B\,(h\nu - E_g) \tag{3}$$

where $h\nu$ is the photon energy, and B is the energy-independent constant.

Meanwhile, the electrical characteristics were measured with a two-probe current-voltage (I-V) method using a manual prober ST103A in the voltage range of -10 to 10 V. The resistance (R) of the samples was determined through Ohm's law as shown in (4).

$$R = \frac{V}{I} \tag{4}$$

The resistivity (ρ) of both samples was calculated from the I-V measurement plots using the equation:

$$\rho = \frac{RA}{t} \tag{5}$$

where A is the surface area of the electrode, and t is the thickness of the sample. Conductivity (σ) was determined using formula (6). Determining conductivity is crucial in order to assess the effectiveness of the sensitivity of the samples [15].

$$\sigma = \frac{1}{\rho} \tag{6}$$

A silver (Ag) electrode was utilized during the electrical measurement. The Ag electrode was deposited with a uniform thickness of 60 nm using an electron beam thermal evaporation system model Ulvac VPC-1100.

3 Results and Discussion

3.1 Surface morphology and cross-sectional images

Fig. 1 (a) and (b) demonstrate cross-sectional views of undoped and Li-doped NiO at 5,000× magnification. Meanwhile, Fig. 1 (c) and (d) display the surface morphologies of the samples magnified at 10,000×. The observation shows that nanosheet and nano coral reef-like (CR) layers have been formed onto the NiO TF. The growth of CR is scattered and not uniform. Both undoped and doped samples have similar nanostructures with no significant differences. This structure is observed as in the previous study, where the same immersion method was used [12]. The only difference between the two samples is their nanosheet and CR thickness. The CR layers of undoped and Li-doped NiO have an average thickness between 4.5 to 11.8 µm. Meanwhile, the thickness of the nanosheet for undoped is 595 nm, while for Li-doped, it has a slightly thicker of 620 nm.

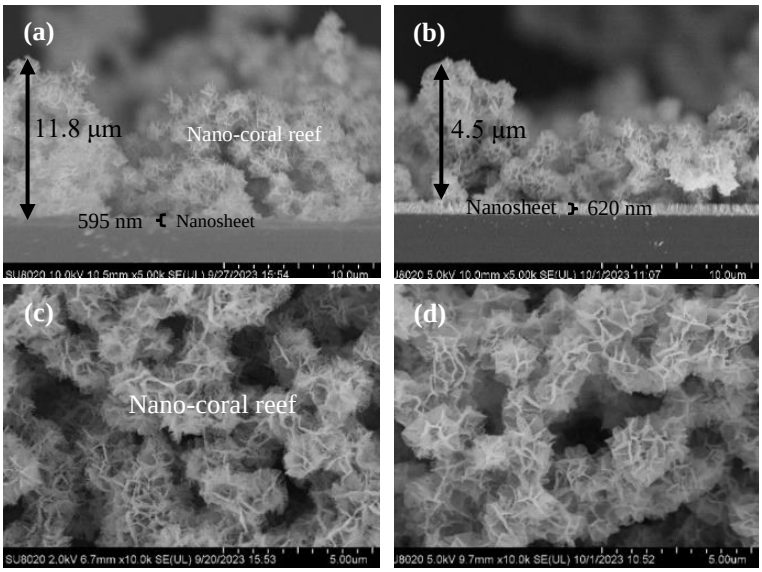

Fig. 1. Cross-sectional images of (a) undoped NiO and (b) Li-doped NiO at a magnification of 5,000×, and surface morphologies of (c) undoped NiO and (d) Li-doped NiO at a magnification of 10,000×.

3.2 Structural properties

NiO CR structures displayed polycrystalline structures that belonged to the face-centered cubic (FCC) NiO phase space group JCPDS card No. 47-1049. The XRD patterns were examined in the 2θ range of 20 - 90°, as demonstrated in Fig. 2. The undoped and Li-doped NiO shows five diffraction peaks at approximately 37.7°, 43.3°, 62.9°, 75.5°, and 79.4°, which were indexed to (111), (200), (220), (311), and (222) crystal planes. However, the Li-doped NiO has three additional diffraction peaks with low intensity, corresponding to the 44.5°, 51.9°, and 76.4°, which were indexed to (220), (131), and (144) crystal planes. It shows the apparent Li in the sample. It was found from the graph that both samples have clear and sharp diffraction peaks, indicating good crystalline quality. At the same time, the intensities of these peaks increased significantly when the NiO sample was doped with Li. As a result, Li-doped NiO CR showed higher intensities in the diffraction peaks and belonged to better crystalline quality than undoped NiO.

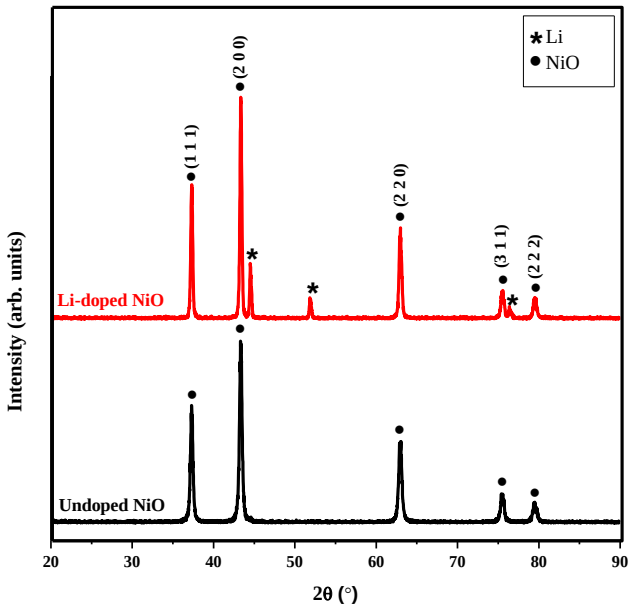

Fig. 2. XRD patterns of the undoped and Li-doped NiO CR structures.

Table 1 presents the crystal properties of undoped and Li-doped NiO CR evaluated at the most prominent crystal plane (200). The 2θ values indicate that the Li-doped NiO diffraction peak is higher and a narrower FWHM than the undoped NiO. Meanwhile, the dislocation density (δ) of undoped NiO is relatively high. The excessive value of 14.284×10^{14} lines/m^2 on the undoped sample showed the loss of its crystalline structure and low crystal quality. In contrast, the Li-doped sample performed the best crystal quality due to the lower δ value. The addition of Li^+ ions to NiO changes its crystalline structure, resulting in a more organized lattice with fewer defects [16]. This alteration reduces the dislocation density in comparison to undoped NiO. Li^+ ions are smaller in size than Ni^+ ions, and when they are added to the NiO lattice, they take up the spots that were initially reserved for NiO ions. This substitution can cause distortions in the lattice, modify the crystal structure, and improve its quality.

On the other hand, the interplanar spacing (d) and lattice parameter (a) values for the undoped NiO exhibit more lattice expansion than Li-doped NiO, which in turn causes the

unit cell volume (V) to indicate a higher value. The strain (ε) for the undoped sample showed a positive value, considered tensile strains. Meanwhile, the Li-doped sample showed a negative value that carries the meaning of compressive strain. For the stress (σ) evaluation, the undoped sample showed a negative value considered compressive stress. Meanwhile, Li-doped samples showed a positive value regarded as tensile stress. The difference in ionic radii between Li^{+} and Ni^{2+} ions is also the cause of changes in strain and stress behavior [17]. This happens because the internal distortion in the host lattice interferes with the crystalline nature of NiO. This disorder stimulates the formation of defects in the Li-doped NiO CR, leading to a change in the behavior of tensile and compressed strain, as well as compressed and tensile stress.

The D values of the five crystal planes of the samples were calculated and recorded in Table 2. The results show that the average D value of Li-doped NiO is higher than the undoped sample, with values of 31.19 nm and 24.70 nm, respectively. The decrease in dislocation density and strain, as well as the increase in stress, has explained the increase in crystalline size.

Table 1. Crystal parameters at (200) plane.

Sample	2θ (°)	FWHM, β (°)	Dislocation Density, δ ($\times 10^{14}$ lines/m^2)	Interplanar Spacing, d (Å)	Lattice Parameters, a (Å)	Unit Cell Volume, V ($\times 10^{-29}$ m^3)	Strain, ε (%)	Stress, σ (GPa)
Undoped NiO	43.300	0.3377	14.284	2.090	4.1796	7.30	6	-0.19
Li-doped NiO	43.337	0.2475	7.671	2.088	4.1762	7.28	-2	0.07

Table 2. The average crystallite size at (111), (200), (220), (311), and (222) planes.

Sample	Crystallite Size, D (nm)					Average D (nm)
	(1 1 1)	(2 0 0)	(2 2 0)	(3 1 1)	(2 2 2)	
Undoped NiO	25.5	26.5	24.1	26.4	21.0	24.7
Li-doped NiO	33.5	36.1	30.0	29.9	26.4	31.2

3.3 Optical properties

Fig. 3 displays the transmittance spectra of both samples in the wavelength ranges of 300 to 800 nm. The Li-doped NiO sample has a higher average transmittance percentage (ATP) than the undoped NiO sample, with 53% and 40%, respectively. The percentage values are calculated within the 400 - 800 nm wavelength range. The presence of a dopant element impacts the transmittance of the samples, as evidenced by the increase in ATP when lithium is doped into the NiO sample. The increase in the ATP was related to the increase in the crystallite size [18]. Large crystallites have fewer grain boundaries and less surface area, resulting in less scattering and more light transmission through the material. The higher ATP may also be affected by an increase in the thickness of the material [19]. Thicker materials allow light to travel through a longer path length, particularly in the visible light spectrum. This extended path length creates more chances for the light to scatter and reflect internally, resulting in a higher percentage of the incident light being transmitted. The average transmittance percentage of the samples is recorded in Table 3.

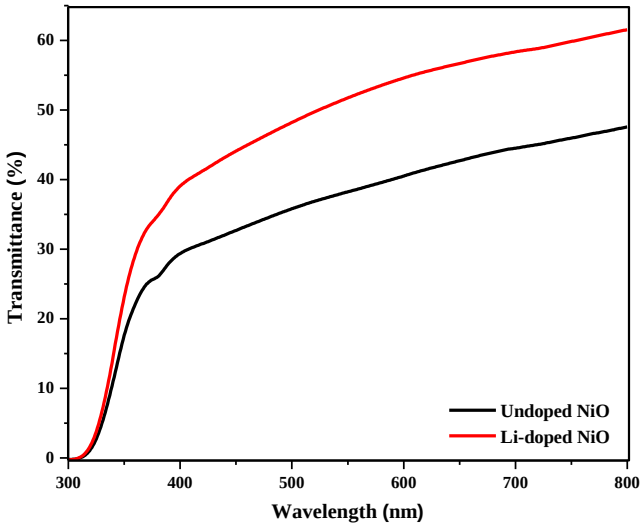

Fig. 3. Transmittance of undoped and Li-doped NiO CR structures.

Table 3. The average transmittance percentage and optical band gap of the samples.

Sample	Average Transmittance (%)	Optical Bandgap, E_g (eV)
Undoped NiO	40	3.94
Li-doped NiO	53	3.95

Fig. 4 shows Tauc's plot, plotted to estimate the E_g of the samples. The values obtained are presented in Table 3. The E_g values were gained from the linear line graph of $(\alpha hv)^2$ versus photon energy (hv), and the estimated values for undoped NiO and Li-doped NiO are 3.94 eV and 3.95 eV, respectively. Based on the results, the E_g values of the samples fall within the range of 3.6 – 4.0 eV, which is consistent with the literature [20].

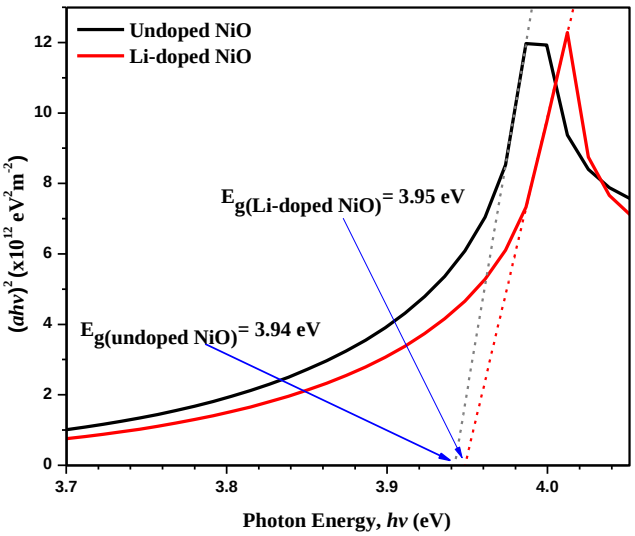

Fig. 4. Tauc's plot for undoped and Li-doped NiO CR structures.

3.4 Electrical properties

The I-V measurement plots of undoped NiO and Li-doped NiO CRs are shown in Fig. 5 with the voltage supply from -10 to 10 V. Both samples exhibit Ohmic characteristics, as linear plots were obtained. The plots indicate that the current value concerning the supplied voltage for the Li-doped NiO increases compared to the undoped.

The calculated R, ρ, and σ of the samples are summarized in Table 4. The results show that the conductivity of the samples increases with the addition of Li elements, as compared to undoped NiO with the values of 7.71 x 10^{-2} S.m^{-1} and 7.90 x 10^{-2} S.m^{-1} for undoped and Li-doped NiO, respectively. This result matches the findings of the previous study, which states that the conductivity of Li-doped NiO should be higher than the undoped NiO sample [21]. The results gained are also affected by the thickness of the CR structures. Sta et al. conducted research on different layers of Li-doped NiO thin film and found that resistivity increases with the increase in thin film thickness [22].

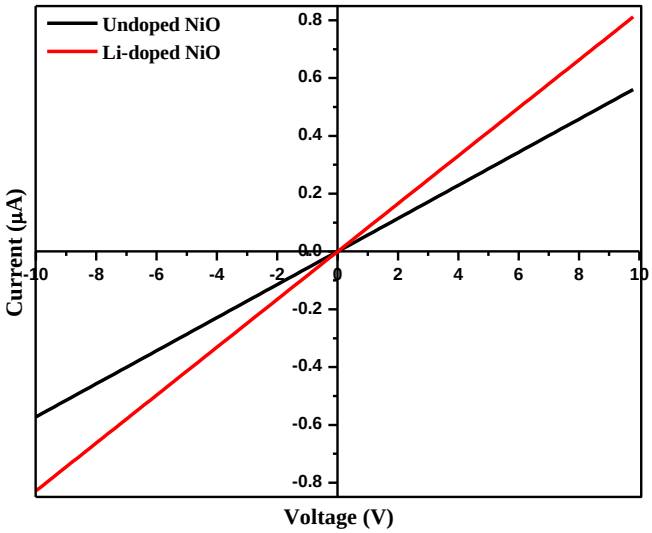

Fig. 5. I-V plot for undoped and Li-doped NiO CR structures.

Table 4. Electrical properties of the undoped and Li-doped NiO CR structures.

Sample	Resistance, R (MΩ)	Resistivity, ρ (Ω.m)	Conductivity, σ (× 10^{-2} S.m^{-1})
Undoped NiO	15.28	13.0	7.71
Li-doped NiO	14.31	12.7	7.90

4 Conclusion

The undoped and Li-doped NiO CR structures were successfully synthesized using a 95 °C immersion approach on NiO thin film. Significant differences exist between them regarding their morphological, structural, optical, and electrical properties. Li-doped NiO is slightly thicker and more crystalline than undoped NiO. In addition, the average crystallite size for Li-doped is larger than undoped. The optical band gap values calculated from Tauc's plot for both samples fall within the general band gap for NiO. The conductivity of Li-doped NiO

CR is higher than the undoped sample. In conclusion, the electrical properties of NiO could be improved with the cooperation of Li as the dopant element. Thus, it is promising in optimization in certain applications, such as a smart window material that can change color and transparency in response to an applied voltage.

References

1. N. P. Klochko, K. S. Klepikova, D. O. Zhadan, S. I. Petrushenko, V. R. Kopach, G. S. Khrypunov, V. M. Lyubov, S. V. Dukarov, V. O. Nikitin, M. O. Maslak, A. Y. Zakovorotniy, A. L. Khrypunanova, Structure, optical, electrical and thermoelectric properties of solution-processed Li-doped NiO films grown by SILAR. Mater Sci Semicond Process. **83**, 42-49 (2018)
2. J. Pan, C. Sun, J. Liu, X. Zhao, C. Jiao, C. Wang, Q. Wang, One-step synthesis method of flower-like Si@NiO/rGO composites as high-performance anode for lithium-ion batteries. J Alloys Compd. **947**, 169506 (2023)
3. K. O. Ukoba, A. C. Eloka-Eboka, F. L. Inambao, Review of nanostructured NiO thin film deposition using the spray pyrolysis technique. Renewable and Sustainable Energy Reviews. **82**, 2900-2915 (2018)
4. S. Kandpal, I. Ezhov, M. Tanwar, D. Nazarov, D. Olkhovskii, L. Filatov, M. Maximov, R. Kumar, Plasma assisted atomic layer deposition NiO nanofilms for improved hybrid solid-state electrochromic device. Opt. Mater. (Amst). **136**, 113494 (2023)
5. M. Ghosh, K. Biswas, A. Sundaresan, N. R. Rao, MnO and NiO nanoparticles: synthesis and magnetic properties. J. Mater. Chem. **16**, 106-111 (2006)
6. B. Wang Y. Huang. S. Zhao, R. Li, D. Gao, H. Jiang, R. Zhang, Novel self-assembled porous yolk-shell NiO nanospheres with excellent electrochromic performance for smart windows. Particuology. **84**, 72-80 (2024)
7. R. Ahmed, G. Nabi, Enhanced electrochemical performance of Cr-doped NiO nanorods for supercapacitor application. J. Energy Storage. 33 (2021)
8. P. Dubey, N. Kaurav, R. S. Devan, G. S. Okram, Y. K. Kuo, The effect of stoichiometry on the structural, thermal, and electronic properties of thermally decomposed nickel oxide. RSC Adv. **8**, 5882-5890 (2018)
9. J. Wang, L. Wei, L. Zhang, J. Zhang, H. Wei, C. Jiang, Y. Zhang, Zinc-doped nickel oxide dendritic crystals with fast response and self-recovery for ammonia detection at room temperature. J. Mater. Chem. **22**, 20038 (2012)
10. A. A. A. Ahmed, E. A. A. Alahsab, A. M. Abdulwahab, The influence of Zn and Mg doping on the structural and optical properties of NiO nanostructures for optoelectronic applications. Results Phys. 22 (2021)
11. P. Sahoo, A. Sharma, S. Padhan, R. Thangavel, Cu doped NiO thin film photocathodes for enhanced PEC performance. Superlattices Microstruct. 159 (2021)
12. N. Parimon M. H. Mamat, K. Ahmad, I. B. Shameem Bahu, M. Rusop, Highly porous NiO nanoflower-based humidity sensor grown on seedless glass substrate via one-step simplistic immersion method. Int. J. Eng. Adv. Technol. **9**, 5718-5722 (2019)
13. P. Sakthivel, G. A. Babu, M. Karuppiah, S. Asaithambi, V. Balaji, M. Pandian, P. Ramasamy, M. Mohammed, N. Navaneethan, G. Ravi, Electrochemical energy storage applications of carbon nanotube supported heterogeneous metal sulfide electrodes. Ceram. Int. **48**, 6157-6165 (2022)

14. A. M. El Sayed, Exploring the morphology, optical and electrical properties of nickel oxide thin films under lead and iridium doping. Phys. B. Condens. Matter. 600 (2021)
15. A. A. Ahmed, N. Afzal, M. Devarajan, S. Subramani, Structural, morphological, optical, and electrical properties of NiO films prepared on Si (100) and glass substrates at different thicknesses. Mater. Res. Express. **3**, 116405 (2016)
16. T. Ungar, Dislocation densities, arrangements, and character from X-ray diffraction experiments. Mater. Sci. and Eng. **309**, 14-22 (2001)
17. M. H. Mamat, N. Parimon, A. S. Ismail, I. B. S. Basha, S. S. Basha, G. V. Vajayaraghvan, M. K. Yaakob, A. B. Suriani, M. K. Ahmad, M. Rusop, Structural, optical, and electrical evolution of sol-gel-immersion grown nickel oxide nanosheet array films on aluminium doping. J. Mater. Sci: Mater. In Electronics. **30**, 9916-9930 (2019)
18. C. C. Diao, C. Y. Huang, C. F. Yang, C. C. Wu, Morphological, optical, and electrical properties of p-type nickel oxide thin films by nonvacuum deposition. Nanomaterials. 10 (2020)
19. A. Samavati, H. Nur, A. F. Ismail, Z. Othaman, Radio frequency magnetron sputtered ZnO/SiO2/glass thin film: Role of ZnO thickness on structural and optical properties. J. Alloys. Compd. **671**, 170-176 (2016)
20. M. H. Mamat, N. Parimon, A. F. Ismail, I. B. Shameen Banu, S. Sathik Basha, R. A. Rani, A. S. Zolfakar, M. F. Malek, A. B. Suriani, M. K. Ahmad, M. Rusop, Syntheis, structural and optical properties of mesostructured, X-doped NiO (x = Zn, Sn, Fe) nanoflake network films. Mater. Res. Bull. 127 (2020)
21. N. Parimon, M. H. Mamat, M. Rusop, Synthesis and Properties of NiO nanosheet array films on glass substrates via immersion technique. Recent Trends in Manufacturing and Mater. Towards Industry. 633-644 (2021)
22. I. Sta, M. Jlassi, M. Hajji, H. Ezzaouia, Structural, optical, and electrical properties of undoped and Li-doped NiO thin films prepared by sol-gel spin coating method. Thin Solid Films. **555**, 131-137 (2014)

Acknowledgments

The authors want to thank the Ministry of Higher Education (MOHE) for financial support under the Fundamental Research Grant Scheme (FRGS/1/2022/TK09/UMS/03/2) and the NANO-ElecTronic Centre (NET) at the School of Electrical Engineering, College of Engineering, UiTM Shah Alam, for the laboratory facilities provided.